Computer simulation of reaction plane memory via quasiparticle dynamics

David H. Boal and John C. K. Wong
Department of Physics, Simon Fraser University, Burnaby, British Columbia, Canada V5A 1S6
(Received 18 September 1989)

Quasiparticle dynamics, a computer simulation for nuclear reactions, is used to investigate reaction plane memory in intermediate-energy heavy-ion collisions. In particular, extensive simulations involving the generation of more than 20 000 events are performed for $^{14}N+^{154}Sm$ at $35A$ MeV. The gamma-ray circular polarization, as a function of trigger mass, energy, and angle, is shown to be a measure of the correlation between the trigger plane and the reaction plane. Calculations of the inclusive particle spectrum, as well as the polarization, are compared with experiment. The dependence of the calculated observables on the assumed in-medium nucleon-nucleon cross section is also investigated.

I. INTRODUCTION

Experimental studies of the space-time history of a nuclear reaction are complicated by many factors: for example, the initial conditions involve an average over impact parameter, and the observed products are the result of a time integration over the collision history. A considerable amount of effort has gone into finding experimental observables that are sensitive to the impact parameter—both its magnitude and direction. One aspect of this problem is the determination of the reaction plane, defined by the impact-parameter vector and the beam direction. In intermediate-energy reactions, observables such as fission-fragment correlations and gamma-ray polarizations have been used as reaction plane indicators.[1]

In one such study,[2,3] the circular polarization of gamma rays emitted in coincidence with a light fragment was measured for two heavy-ion reactions at intermediate energy. It was found that the polarization generally tended to increase with trigger fragment mass and energy. With a few simple assumptions, the data were interpreted as showing that for a range of fragment masses and energies, particle emission tended to occur in a direction opposite to the direction of the impact-parameter vector.

The space-time histories of nuclear reactions are further complicated by decay processes, which have a much longer time scale than the initial reaction time scale. Hence, it is important to determine how good an observable's "memory" is of the initial variable of interest. Computer simulations have proven to be an important tool in this evaluation. Simulations allow one to follow the time evolution of a reaction from specified initial conditions, and investigate how an observable changes during the collision process. They also allow one to vary quantities otherwise beyond the experimentalist's control, such as the strength of the nuclear force, and examine the role of such quantities in determining the outcome of a collision.

The polarization experiment mentioned earlier has been analyzed[2,3] through the use of a simulation of the one-body distribution of nucleons. The simulation, known as the Boltzmann-Uehling-Uhlenbeck (BUU) model,[4] incorporates both a nuclear mean field as well as a stochastic nucleon-nucleon (NN) collision term. A number of assumptions must be made in order to extract fragments from the one-body distributions, and a procedure must be adopted for predicting the gamma-ray emission from these fragments. The simulation was used to predict the polarization for nucleon triggers, as well as the dependence of the polarization on the assumed in-medium NN cross section.

In the time since the original calculations were performed, a considerable amount of effort[5–7] has gone into developing simulations for many-particle distributions. These simulations include correlations between nucleons, and so incorporate fragment emission without further assumptions. One such model is the Quasiparticle Dynamics model[6] (QPD), which is Hamiltonian-based, yet includes a stochastic NN collision term.

In this paper, QPD will be used to simulate the polarization experiment of Refs. 2 and 3 for the reaction N+Sm at $35A$ MeV. QPD allows the examination of several effects that could not be included in the original simulation:

(1) QPD is a many-body model in which the correlations between nucleons do not need to be incorporated in a model-dependent fashion.

(2) In BUU-like models the combined effects of the collision term and numerical integration procedure may lead to "ground-state" nuclei that are unstable on the time scale of a few hundred fm/c. Hence, one has to stop the simulation (at 100–200 fm/c) to avoid possible evaporation of the nuclei. In QPD, the nuclei are true ground states of the Hamiltonian governing their equations of motion and this allows the rection to be followed for 1000s of fm/c (the need for this property was emphasized in Ref. 7). Hence, much longer time frame effects can be evaluated with QPD.

(3) Because the nuclei are true ground states in QPD, then it is straightforward to determine the quantities such as excitation energy distributions and follow their time evolution.

As will be shown later, the QPD results qualitatively

support the earlier BUU calculations, even though many of the assumptions necessary in the earlier work are not required in QPD. However, the polarization is found to be quantitatively larger than was calculated previously, and larger than is observed experimentally.

The paper is organized as follows: Section II contains a very brief review of the QPD model and some technical issues that are relevant to the numerical work that follows. Section III contains a comparison of the QPD predictions for inclusive cross sections of the N+Sm reaction at 35 A MeV with the experimental data. Since there is some question regarding the magnitude of the effective in-medium NN cross section to be used in the simulations, results will be shown for two choices of the cross section: 28 and 60 mb (the lower cross section is what was used in the original formulation of the model). A limited comparison will be made in this section with results from a recent BUU simulation[8] of the N+Sm reaction at 35 A MeV.

The polarization results are presented in Sec. IV. This section contains a comparison with the data and an investigation of the relationship between the polarization and the orientation of the reaction plane with respect to the trigger plane. Section V contains a discussion of our findings and of the effects of long time frame decays.

II. NUMERICAL DETAILS

In the Quasiparticle Dynamics model, each nucleon is represented by a Gaussian wave packet of characteristic size $1/\alpha$ in coordinate space. Computer time limitations do not permit us to evolve the widths with time; they are assumed to be fixed. The degrees of freedom for the equations of motion are then taken to be $\langle x \rangle$ and $\langle p \rangle$, the expectations of the individual wave packets. Hence, each nucleon is represented by a quasiparticle whose phase-space coordinates $\mathbf{R}$ and $\mathbf{P}$ are $\langle x \rangle$ and $\langle p \rangle$, respectively.

However, these wave packets are not used to form an antisymmetric wave function. Instead, a momentum-dependent potential acting pairwise between the quasiparticles is used to incorporate many of the effects on the fermions' energies arising from antisymmetrization. This potential between quasiparticles a and b has the form

$$V_p(X_{ab}) = V_s \frac{\alpha^2 \hbar^2 X_{ab}}{2m(e^{X_{ab}} - 1)} , \tag{1}$$

where

$$X_{ab} = \tfrac{1}{2}[\alpha^2(\mathbf{R}_a - \mathbf{R}_b)^2 + (\mathbf{P}_a - \mathbf{P}_b)^2/(\hbar\alpha)^2] , \tag{2}$$

and m is the nucleon mass. The two parameters in Eqs. (1) and (2) are fixed by the demand that in the absence of other interactions, a system of quasiparticles obeying Eq. (1) has the energy of an ideal gas of fermions over the range of densities of interest. The complete Hamiltonian of the system also includes terms representing the (isospin dependent) nuclear interaction as well as the Coulomb interaction. Hamilton's equations are then used to govern the time dependence of $\mathbf{R}$ and $\mathbf{P}$ for each quasiparticle.

This dynamics is supplemented by the use of a stochastic collision term between nucleons. In many BUU-based models, the collision term is handled in the following manner: an in-medium NN cross section σ_{NN} is used to define a classical radius R_{NN} such that if the distance of closest approach of two approaching nucleons is less than this radius, a collision is tentatively assumed to have occurred (subject to Pauli exclusion principle considerations). The directions of the nucleons' momenta after the collision is randomly selected from a predetermined distribution (usually assumed to be isotropic in the c.m. frame at these collision energies). The magnitudes of the momenta are determined from conservation of energy and momentum.

In such a prescription, there is no relationship between the impact parameter of the NN collision and the pair's relative momentum after the collision; the procedure does not conserve angular momentum. In simulations of one-body distributions, it does not matter whether angular momentum is conserved on an "event-by-event" basis so long as the distribution determined by averaging over events does conserve angular momentum. In QPD, each event is taken to be an independent realization of a nuclear collision. Nonconservation of angular momentum then has catastrophic consequences; cold nuclei spontaneously acquire angular momentum. Hence, in QPD a collision algorithm is adopted that is both stochastic and conserves angular momentum. In essence, what happens is that the collision point is randomly chosen from a predetermined distribution, but all conservation laws are then applied to the collision. Further details on the form of the interaction and the collision term can be found in Ref. 6.

The equations of motion of the quasiparticles are integrated using a Runge-Kutta procedure. We find that the momenta and excitation energies of the reaction products stabilize by about 150 fm/c elapsed time in the reaction where the collision begins about 20 fm/c after the simulation is started. Each event is propagated for a total of 250 fm/c elapsed time and takes about 4 cpu minutes to execute on an IBM 3081 computer. The generation of the event sample and its analysis took approximately 1000 cpu h to execute.

For the reaction N+Sm at 35 A MeV, a total sample of 14 720 events is generated over the impact-parameter range 0.5–7.5 fm in 1 fm steps. The number of events per impact parameter is determined by its areal weighting. This large sample has a value of σ_{NN} of 28 mb. A second data set of 6400 events is also reported for σ_{NN} of 60 mb. These comparatively large event samples are required because of the trigger condition used in the experimental studies: we wish to be able to study the inclusive spectra as well as the polarization as a function of trigger fragment mass, energy, and angle.

III. SINGLE-PARTICLE INCLUSIVE SPECTRA

The single-particle spectra are calculable in a straightforward manner. Each initialization in the simulation is propagated for 250 fm/c, at which time a cluster search is made over all nucleon positions. In the search, nucleons which are less than 3.5 fm apart are linked together to

form clusters. The clusters that are produced by this definition are not usually in their ground states at this point in the reaction sequence. However, they are stable on the time frame of 1000 fm/c, a fact to which we will return later. In other words, the clusters retain their integrity over a longer time frame than that for which it is computationally economical to run the simulation.

The question that is addressed in this section is how well does the simulation agree with the single-particle inclusive measurements? The predicted spectra show the usual behavior: in the lab frame there is a roughly exponential falloff with emission energy at fixed angle, and a decrease with angle at fixed energy. An example of a comparison of the predictions with experiment is shown in Fig. 1. The spectra shown are for proton emission at 30° and 60°. These two angles are the ones used in the experiment and are representative of the data set of the simulation. The predictions are indicated by the histograms; the dashed curve is for $\sigma_{NN}=28$ mb, while the solid curve is for 60 mb. At wide angles, the two in-medium cross sections give similar results, while at forward angles, the larger in-medium cross section yields a smaller inclusive cross section at proton energies of the order of the beam energy per nucleon.

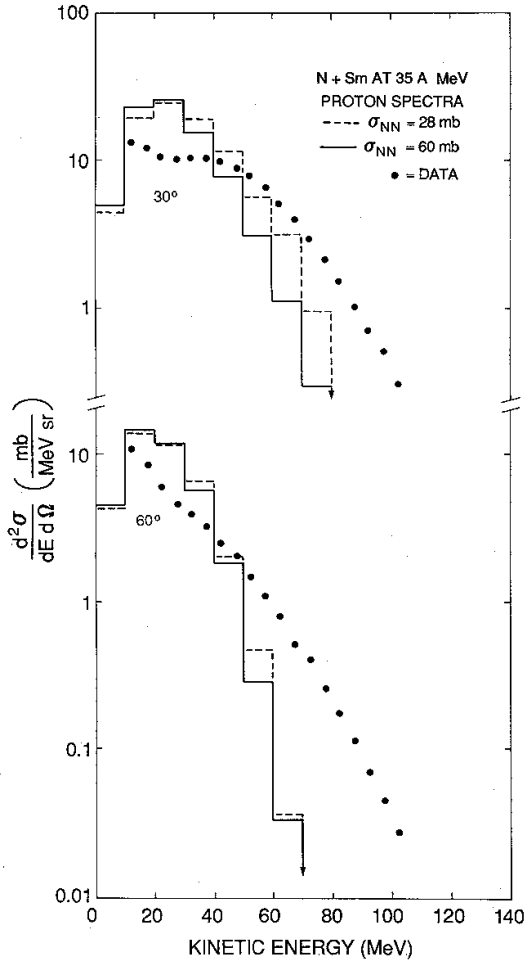

FIG. 1. Comparison of data (from Refs. 2 and 3) with QPD predictions for proton emission in N+Sm at 35A MeV. The data are shown as the circles, while the predictions are the histograms (dashed curve for $\sigma_{NN}=28$ mb and solid curve for 60 mb).

This dependence on σ_{NN} is found not just for proton emission, but for clusters as well. In Figs. 2 and 3, comparisons are made of the predicted and measured inclusive deuteron and triton spectra, respectively. While the statistics are not as good as the proton spectrum, nevertheless the smaller σ_{NN} corresponds to the larger inclusive cross section at forward angles and fragment kinetic energies per nucleon of the order of the beam energy per nucleon. However, the energy integrated angular distributions do not show a particularly strong dependence on the in-medium cross section. This can be seen from Table I, in which the differential cross sections from Figs. 1–3 (plus the alpha-particle spectrum) are integrated to give a fragment multiplicity as a function of angle. Results are shown for both 28 and 60 mb cross sections.

It should be pointed out that this particular dependence of the inclusive cross section on σ_{NN} may be peculiar to this energy range. In simulations that we have performed for zero impact-parameter La+La collisions at 250A MeV we find that the wide angle cross section increases with σ_{NN}. The magnitude of the increase depends on target and projectile mass: the effect is much less pronounced for Ag+Ag than for La+La.

These results may appear to be somewhat surprising, taken at face value. What appears to be happening is

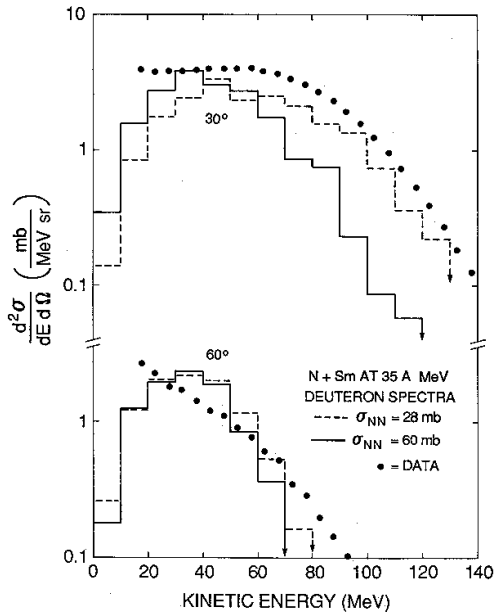

FIG. 2. Similar to Fig. 1 but for deuteron emission.

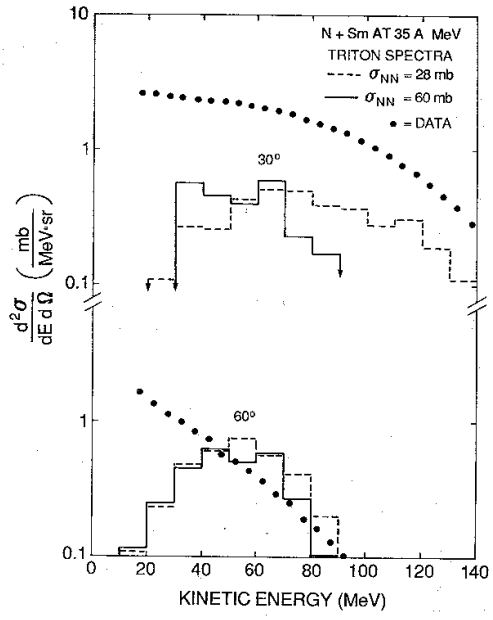

FIG. 3. Similar to Fig. 1 but for tritium emission.

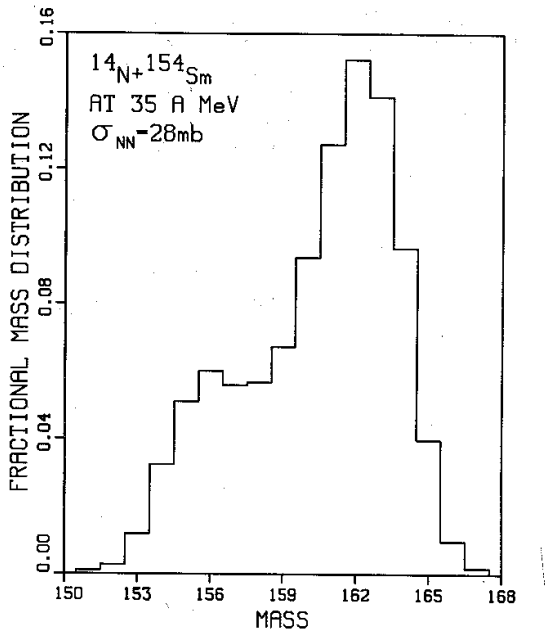

FIG. 4. Predicted heavy nucleus mass yields for N+Sm at 35A MeV, averaged over impact parameter and integrated over fragment energy and angle. The yields are calculated after an elapsed time of 250 fm/c. The distribution is normalized to unity over the fragment mass range shown.

that the motion of the nucleons is becoming more thermalized at higher values of σ_{NN}, as one would expect. In other words, the population of nucleons with kinetic energy in the range of the beam energy per nucleon is being reduced by scattering. Further, these nucleons are trapped in excited residual nuclei that do not decay on the time scale of the simulation.

To investigate the magnitude of the excitation energy of the residual reaction products, we first examine the mass distribution of the products. This is shown in Fig. 4 for $\sigma_{NN}=28$ mb. The distribution is averaged over impact parameter, integrated over fragment emission energy and angle, and normalized to unity over the mass range shown (there is very little change in the probabilities if the normalization condition is removed). There is an obvious peak in the mass distribution at a value greater than the target mass of $A=154$, meaning that some of the mass of the projectile has been transferred to the target.

Suppose now we take a particular nucleus near the peak of the distribution and evaluate its average excitation energy. As an example, we choose the computational ^{163}Ho nucleus, whose ground-state energy is -8.34 MeV (this must be calculated separately; see Ref. 6 for methodology). The fractional distribution in excitation energy for this nucleus is shown in Fig. 5, where the same integrations, averages and normalization are chosen as in Fig. 4. Clearly, there is a spread in excitation energies, with the peak in the distribution falling below $2A$ MeV. We find that the average excitation energy is 1.85 and 1.98A MeV for $\sigma_{NN}=28$ and 60 mb, respectively. Hence, we conclude that there is still a substantial amount of excitation energy in the residual systems and that the larger in-medium cross section leads to somewhat greater thermalization of the bombarding energy.

Figures 1–3 are encouraging in that the predictions of the simulation are generally within a factor of 2 of experiment. Given the approximations of the model, and that long time evaporative decays are not included in the model, the agreement is as one would expect. However, the experimental data do not necessarily favor one particular value of σ_{NN}. Although the 28 mb predictions appear to be in better agreement with the data for high-energy particles emitted at forward angles, this kinematic region may be one in which the internal Fermi momentum of the projectile nucleons plays a role. The model was not designed to calculate the high momentum components of the nuclear wave function, and so we prefer not to use this comparison as a test of the in-medium cross section.

TABLE I. Differential multiplicities of the trigger fragments at different combinations of emission angle and in-medium NN cross section.

Angle	σ_{NN} (mb)	p	d	t	^{4}He
30°	28	0.44	0.097	0.020	0.015
30°	60	0.41	0.089	0.014	0.011
60°	28	0.19	0.048	0.017	0.015
60°	60	0.19	0.044	0.018	0.011

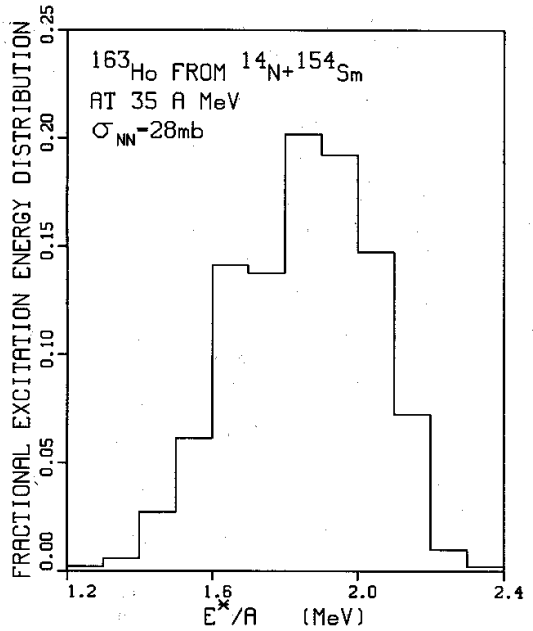

FIG. 5. Predicted fractional distribution of excitation energy for the ^{163}Ho nucleus calculated from the simulation of N+Sm at 35A MeV, as in Fig. 4. The excitation energy is calculated after an elapsed reaction time of 250 fm/c.

It is worthwhile making a comparison between the QPD predictions and those obtained in a recent BUU calculation[8] of the same reaction. We begin with the summed proton and neutron cross sections. BUU calculations do not give the free nucleon spectrum directly; an assumption must be made to extract it from the one-body distribution of nucleons in phase space. A common procedure is to evaluate the local coordinate space density in a region to determine the strength of the nuclear mean field, and from this extract the fraction of nucleons in that region that are unbound. This procedure will give a higher number of free nucleons than what is observed in the QPD simulation, since there is still substantial excitation energy in the residual nuclei at the time when the QPD simulation is stopped. What we find is that while the cross sections predicted by the two models are similar in shape, the QPD results are about a factor of 2–3 lower in magnitude. A similar effect is noticed in the mass yield of heavy residual nuclei: the QPD heavy nucleus mass yield at 250 fm/c is peaked at several mass units higher than the BUU one. Given the difference in the definition of the observables in the two codes, the agreement is in the range expected. Lastly, the BUU results for the integrated nucleon cross section do not show strong sensitivity to σ_{NN} in the 20–41 mb range, similar to what is found in QPD.

IV. POLARIZATION CALCULATIONS

The QPD model itself does not include a mechanism for dealing with gamma-ray emission. What it provides us with are the positions, momenta, excitation energies, and angular momenta of clusters at any time during the collision. In order to calculate the polarization, we use the model advanced in Ref. 2, in which gamma emission is assumed to be 100% stretched $E2$ transitions of the heavy residual nuclei. Such transitions have a gamma-ray multiplicity of $M_\gamma = J/2$ for a nucleus with angular momentum J. For each simulation event, there is generally only one large residual nucleus present, and its angular momentum vector is used to calculate the characteristics of the emitted gammas.

The labeling convention for the vectors involved in the polarization calculation is as follows: The momenta of the trigger fragment and the beam are used to define a trigger plane. The initial reaction plane, defined by the beam direction and the impact-parameter vector **b** lies at an angle θ with respect to the trigger plane. That is, we have adopted the convention that if **b** points in the same direction as the transverse component of the trigger momentum then θ vanishes.

Experimentally,[9] the polarimeter to measure the gamma-ray polarization is located with its axis perpendicular to the trigger plane, and it subtends a solid angle Ω with respect to the target position. A gamma ray with momentum **k** is emitted from the residual nucleus with an angular distribution given by $Y(\beta)$, where $\cos(\beta)=\mathbf{k}\cdot\mathbf{J}/kJ$. The circular polarization is defined as $P(\beta)$ for a gamma emitted at angle β. The dependence of Y and P on β is given by

$$Y(\beta)=1-\cos^4(\beta) \tag{3}$$

and

$$P(\beta)=\frac{2\cos(\beta)}{1+\cos^2(\beta)} . \tag{4}$$

The polarization measured with a trigger fragment at angle and energy θ,E is given by

$$P(\theta,E)=\frac{\langle M\int d\Omega P(\beta)Y(\beta)\rangle}{\langle M\int d\Omega Y(\beta)\rangle} , \tag{5}$$

where the average is taken over those events satisfying the trigger conditions. The details of the angular integrals can be found in Refs. 2 and 9.

We begin with an overview of the behavior of the calculated polarization. In Fig. 6 we show the dependence of the predicted polarization on fragment trigger mass and kinetic energy. The trigger angle is fixed at 30° and σ_{NN} is chosen to be 28 mb. For clarity, only a few representative error bars are shown on the figure. One can see two trends: the polarization increases with trigger energy and mass. These trends are qualitatively similar to what is observed experimentally. The very large error bars at low trigger energy are the result of the small event sample in that kinematical region.

The dependence of the polarization on trigger angle is shown in Fig. 7 for $\sigma_{NN}=28$ mb. For proton triggers, there is little change in the polarization from 30° to 60° (we do not have sufficient statistics to come to any conclusion at wider angles) and the trigger energy depen-

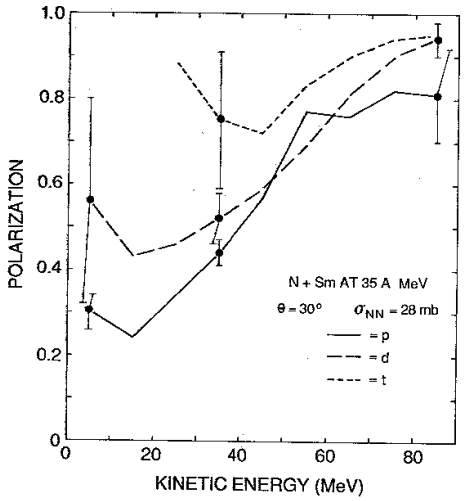

FIG. 6. Predicted trigger mass and energy dependence of polarization for trigger fragments observed at 30°. An in-medium NN cross section of 28 mb is used in the calculation. The results are for the reaction N+Sm at 35A MeV, and are averaged over impact parameter.

dence is similar at both angles. For deuterons, the angular dependence is more pronouced; the polarization increases with angle. Again, these observations are qualitatively the same as what is seen experimentally.

However, the magnitudes that we predict for the polarization are higher than what is observed experimentally, unless the in-medium cross section is very large. In Fig. 8, we show a comparison between data and the simulation for proton triggers. Predictions are shown for two angles (30° and 60°) and two choices of σ_{NN}. Clearly, the larger value for the cross section gives a lower predicted polarization. This is what one would expect: more collisions tend to reduce the angular momentum alignment of the residual nucleus. The effect of increasing σ_{NN} is also seen in deuteron and triton triggers. These results are shown in Fig. 9 for deuterons. Again, even the $\sigma_{NN}=60$ mb prediction shows a larger polarization than is seen in the data.

Let us now use the simulation to examine the microscopic dynamics of the collision process. The fact that the simulation has predicted large values for the gamma-ray polarization leads us to expect that there is a strong correlation between the trigger plane and the reaction plane. We begin our investigation of this question by examining the distribution of impact parameters for a given trigger energy and angle. The trigger plane is used to define the x and z axes of a Cartesian coordinate system;

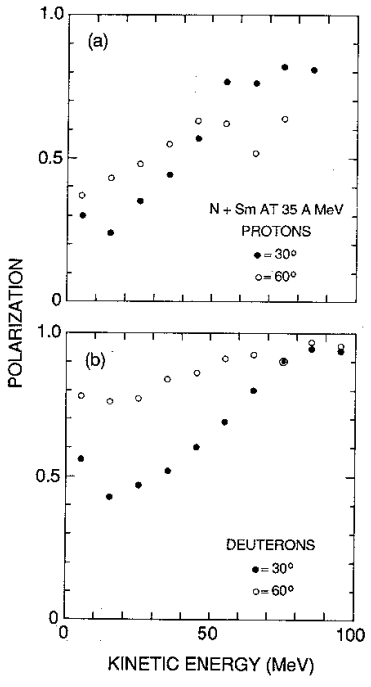

FIG. 7. Predicted trigger emission angle dependence of polarization for proton (a) and deuteron (b) triggers at both 30° and 60°. Other conditions are as in Fig. 6.

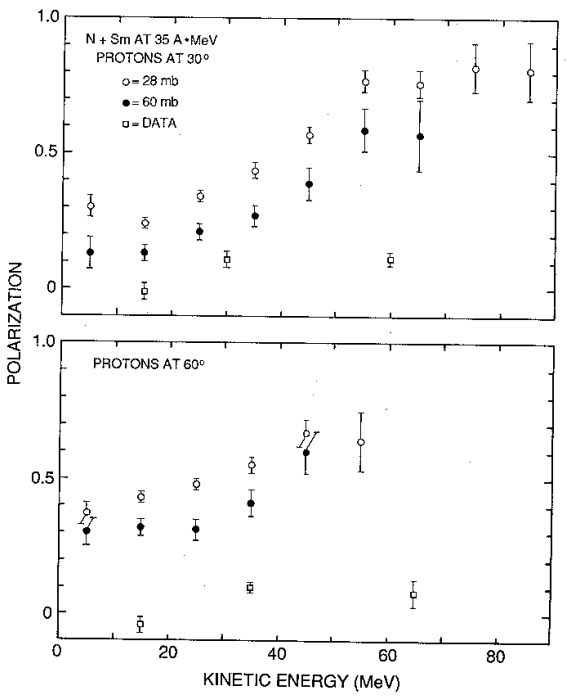

FIG. 8. Comparison of simulation and experiment for proton triggered events at 30° and 60°. Two values of σ_{NN} were used in the simulation : 28 and 60 mb. Data are from Refs. 2 and 3.

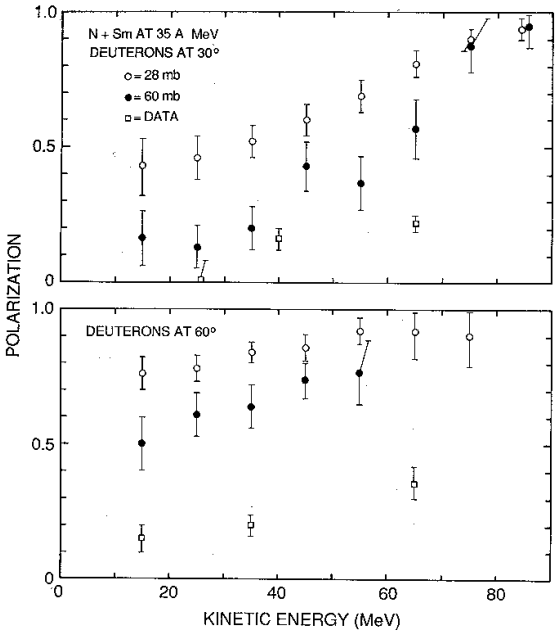

FIG. 9. Similar to Fig. 8 but for deuteron triggers.

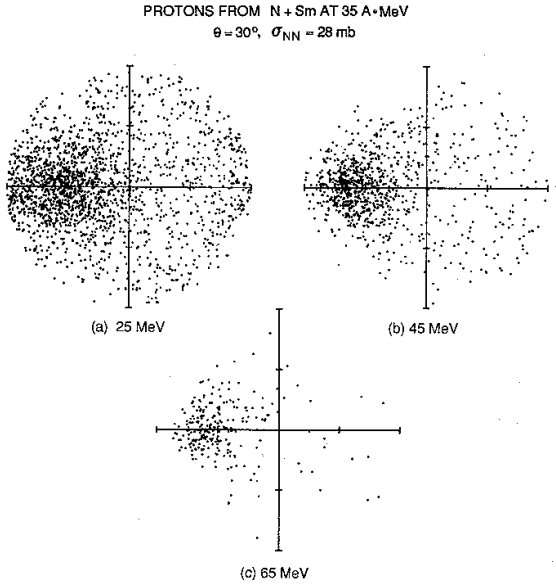

FIG. 10. Distribution of impact-parameter **b** for proton triggers emitted at 30° and a range of energies. The acceptance range of each energy shown is +/− 5 MeV. Cross marks are placed on the axes every 4 fm.

the z axis is defined by the beam direction and the positive x axis is the direction in which lies that component of the trigger momentum that is perpendicular to the beam. The impact-parameter vector then lies in the x-y plane, perpendicular to the beam.

A scatter plot of the impact parameter for proton triggers at 30° is shown in Fig. 10. The plot contains three sections, corresponding to proton kinetic energies of 20–30, 40–50, and 60–70 MeV. The results are taken from the simulation with 28 mb for the *NN* in-medium cross section. In generating the scatter plot, we have shifted the magnitude (but not the direction) of the impact-parameter vector randomly by up to 0.5 fm. This procedure is necessary because the impact parameters used in the code are taken to be 0.5, 1.5, 2.5. . . fm, which results in the data points falling in concentric circles. Hence, we spread the points out in order to more clearly display their density.

At low proton trigger energy, there is a very pronounced enhancement for impact parameters in the opposite side of the beam from the trigger momentum. There also appears to be a small enhancement on the same side as the trigger momentum. The tendency for the trigger to emerge on the opposite side of the beam from the impact-parameter vector becomes stronger with increasing trigger energy, as one can see in comparing parts (a)–(c) of Fig. 10. A more quantitative representation of this effect is presented later.

The tendency for the trigger to emerge on the opposite side of the target from the projectile is not simply confined to proton triggers. Shown in Fig. 11 is a similar scatter plot for deuteron triggers. The conditions are the

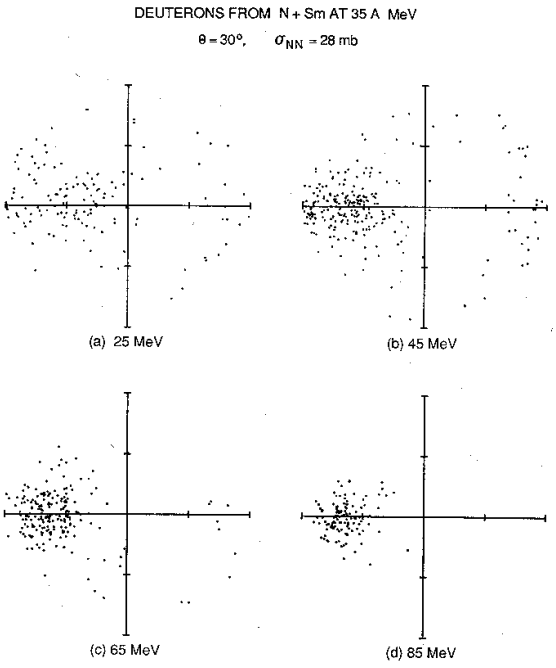

FIG. 11. Similar to Fig. 10 but for deuteron triggers.

same as those used in Fig. 10, except that four kinetic energy ranges are shown: 20–30, 40–50, 60–70, 80–90 MeV. The figure demonstrates that the higher the trigger energy, the stronger the tendency to scatter to the opposite side of the projectile. For both trigger masses, the simulations show that the path of the beam nucleus is bent around the target nucleus as they interact; there is usually some mass transfer to the target and it gains angular momentum. The beam does not, on average, "bounce off" the target at these energies. Similar conclusions to this were reached in Refs. 2 and 3.

To put these conclusions on a more quantitative footing, we evaluate the expectation and dispersion of the angle θ between the reaction plane and the trigger plane. For all cases considered, $\bar{\theta}=\langle\theta\rangle$ is close to 180°, as one would expect. However, the dispersion $\langle(\theta-\bar{\theta})^2\rangle$ around the mean may be substantial. It is oberved that the dispersion decreases with increasing trigger energy and, correspondingly, with polarization. Shown in Fig. 12 is the behavior of the dispersion as a function of the polarization for proton and deuteron triggers at 30° and an in-medium cross section of 28 mb. The figure is constructed by evaluating the dispersion and polarization for the energy bins used in Figs. 6 and 7.

For low values of the polarization, the dispersion tends towards a distribution of impact parameters that is random in the x-y plan. As the polarization increases, the width of the impact-parameter distribution narrows, tending to zero as the polarization tends to unity. This is what one would expect: the more the reaction and trigger planes are coincident, the more the angular momentum vector of the residual nucleus is perpendicular to them. In other words, the simulation shows that the polarization is a good indicator of the correlation between the reaction and trigger planes.

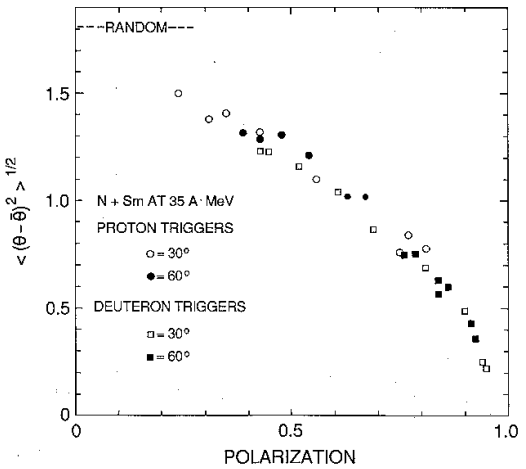

FIG. 12. rms deviation of the orientation of the reaction plane with respect to the trigger plane shown as a function of polarization for both values of σ_{NN} in the simulation.

V. DISCUSSION

In the previous sections, comparisons are made between a simulation based on the QPD model and the experimentally observed inclusive cross section and fragment triggered polarization for N+Sm at 35A MeV. The agreement between the data and the simulation is in the range expected (given the approximations of the model) for the inclusive spectra. A value of 28 mb chosen for the in-medium NN cross section gives better agreement with the data compared to 60 mb, but a hard conclusion cannot be drawn because of uncertainties that may arise from effects that are not incorporated in the model.

For example, the collision is only followed for a time of 250 fm/c. This is long enough to ensure that the clusters are internally thermally equilibrated, but not long enough for them to decay into their ground states by particle or gamma emission. Processes such as evaporation have a much longer time scale than that for which it is practiable to run the simulation. Certainly, long time frame evaporation will boost the yields of light mass particles, and will bring the $\sigma_{NN}=60$ mb predictions in better agreement with the data.

The predicted circular polarizations are in qualitative agreement with the data in terms of trends with respect to fragment trigger mass, energy, and emission angle. However, the predictions are consistently higher than the data. Again, part of the reason for the discrepancy lies in long time decays that will reduce the alignment of the angular momentum vector of the residual nucleus.

To see how large an effect this would be on the time scale of 1000 fm/c, we take a sample of the ^{163}Ho nuclei discussed in Sec. III and propagate them for an extra 1000 fm/c. The change in orientation of the angular momenta is observed to be less than 1%. This demonstrates: (i) that there are few evaporative decays on a time frame that can be handled by the simulation, and (ii) that the simulation conserves angular momentum very well. Hence, we are unable to resolve whether evaporative decays on the time scale of 10^{-19} sec result in substantial dealignment of the residual system.

Trautmann *et al.*[10] have attempted to assess the effect of nonstretched transitions on predictions of the gamma-ray circular polarization. They conclude that a reduction of the polarization in the 10% range could be expected for nuclei in the mass 50 range. It may prove to be the case that this effect along with the dealignment arising from the evaporative decays will eliminate the discrepancy between our predictions and the data. The resolution of these issues needs further effort on both the theoretical side, as outlined earlier, and the experimental side. For example, an experimental investigation using the gamma cascade of the residual nucleus to determine its alignment would provide new information on angular momentum transfer that could be compared with predictions.

In spite of the aforementioned, the agreement between the simulation and experiment is surprisingly good. The central question that we ask of the simulation is whether there is a strong correlation between the polarization and

the distribution of the reaction plane's orientation with respect to the collision plane. The simulation shows that there is indeed a correlation, and that it becomes stronger the closer the polarization is to unity. Further, the impact parameter tends to point in the opposite direction to the trigger direction. This indicates that the long-range nuclear interaction tends to pull the nuclei around one another, although not sufficiently strong enough to result in an orbiting pair at these bombarding energies.

ACKNOWLEDGMENTS

The authors wish to thank J. Glosli for fruitful discussions about error analysis. They also wish to thank M. B. Tsang, W. G. Lynch, and C.-K. Gelbke for many discussions and for providing tabulations of experimental data as well as details of BUU-based calculations. This work was supported in part by the Natural Sciences and Engineering Research Council of Canada.

[1]For a review, see C.-K. Gelbke and D. H. Boal, Prog. Part. Nucl. Phys. **19**, 33 (1987).

[2]M. B. Tsang, R. M. Ronningen, G. Bertsch, Z. Chen, C. B. Chitwood, D. J. Fields, C.-K. Gelbke, W. G. Lynch, T. Nayak, J. Pochodzalla, T. Shea, and W. Trautmann, Phys. Rev. Lett. **57**, 559 (1986).

[3]M. B. Tsang, W. G. Lynch, R. M. Ronningen, Z. Chen, C.-K. Gelbke, T. Nayak, J. Pochodzalla, F. Zhu, M. Tohyama, W. Trautmann, and W. Dunnweber, Phys. Rev. Lett. **60**, 1479 (1988).

[4]G. Bertsch, H. Kruse, and S. Das Gupta, Phys. Rev. C **29**, 673 (1984).

[5]For examples, see C. Gale and S. Das Gupta, Phys. Lett. **162B**, 35 (1985); G. E. Beauvias, D. H. Boal, and J. C. K. Wong, Phys. Rev. C **35**, 545 (1987); J. Aichelin and H. Stocker, Phys. Lett. B **176**, 14 (1986); C. Gregoire *et al.*, Nucl. Phys. **A471**, 399c (1987).

[6]D. H. Boal and J. N. Glosli, Phys. Rev. C **38**, 1870 (1988); **38**, 2621 (1988); see also D. H. Boal, J. N. Glosli, and C. Wicentowich, Phys. Rev. Lett. **62**, 737 (1989).

[7]A. Vincentini, G. Jacucci, and V. R. Pandharipande, Phys. Rev. C **31**, 1783 (1985).

[8]M. B. Tsang, G. F. Bertsch, W. G. Lynch, and M. Tohyama, Michigan State University Report No. MSUNSCL-681, 1989.

[9]W. Trautmann, C. Lauterbach, J. de Boer, W. Dunnweber, G. Graw, W. Hamann, W. Hering, and H. Puchta, Nucl. Instrum. Methods **184**, 449 (1981).

[10]W. Trautmann, W. Dunnweber, W. Hering, C. Lauterbach, H. Puchta, R. Ritzka, and W. Trombik, Nucl. Phys. **A422**, 418 (1984).